ISSN: 2688-8645

Vibration Characteristics Analysis of Gas-Liquid Multiphase Internal Flow Composite Tubing String

Xueping Chang [1], Renqiang Xu [1], Congjia Qu [1], Yinghui Li [2]

[1] School of Mechatronic Engineering, Southwest Petroleum University, Chengdu Sichuan, 610500, China

[2] School of Mechanics and Aerospace Engineering, Southwest Jiaotong University, Chengdu Sichuan, 610031, China

Abstract

This study explores the flow-induced vibration characteristics of composite tubing under the action of gas-liquid multiphase flow. Based on the Hamilton variational principle, the longitudinal-transverse coupling vibration control equation of the pipe string is established, which is solved by the Galerkin method and verified by the benchmark case. The parameter analysis shows that the stability of the system is affected by the internal flow velocity, gas content, fiber ply angle, bottom hole pressure and packer position. It is found that the critical velocity of multiphase flow is significantly higher than that of single-phase flow, and there is a linear relationship between the critical velocity and the gas fraction in a specific void fraction range. The critical velocity curve and natural frequency curve with the change of fiber ply angle show symmetrical distribution. Optimizing the position of the packer can generate extreme points in the critical flow rate and natural frequency, and achieve a synergistic peak of a specific configuration. The comparative analysis shows that the bottom hole pressure is the dominant stability factor, which significantly affects the vibration energy distribution. The numerical analysis data in this paper provide a theoretical basis for offshore oil exploitation and geothermal well application.

Keywords

Flow-induced Vibration; Hamilton Principle; Composite Material Tubing; Gas-Liquid Multiphase Flow.

1. Introduction

The function of tubing in the oil and gas extraction process is obvious since it is the sole conduit that carries gas and oil between the wellhead and the bottom hole. Exploration and development of high temperature and high pressure wells are encouraged by the world's growing need for oil and gas resources. Composite tubing offers numerous mechanical benefits over steel tubing, including reduced weight, resistance to corrosion, improved thermal insulation, and robust fatigue resistance. Consequently, there is a lot of potential for using composite tubing in the construction of oil and gas wells that are subjected to high temperatures and pressures [1]. It is primarily made up of fiber-reinforced laminates, each of which has an outside and inner lining layer for wear resistance and fluid sealing [2].

The tubing string is prone to nonlinear vibration because of the high-speed fluid in the tubing during the oil and gas production process. Along with a host of additional problems, such as fatigue damage to the tubing string, loosening of the downhole tools that match the tubing, and failure of the connecting thread, this can cause alternating load and dynamic stress in the tubing. Operations involved in oil extraction will suffer significant losses if the flow-induced vibration has a considerable amplitude. The dynamic response of the tubing string is also significantly impacted by the increased pipeline instability caused by the multiphase flow in the pipeline[3]. An first investigation into the vibration properties of steel tubing strings was carried out by researchers [4]. The experimental test confirms that the fluid flow in the pipe has a considerable impact on the pipe string's dynamic response [5]. Following a more thorough investigation of the tubing string's vibration model, the fluid force calculation method [6], the tubing string's longitudinal and transverse vibration models [7, 8], and the fluid-solid coupling vibration model [9] were all produced. On this basis, Guo and Liu et al. [10]analyzed the vibration response of high temperature and high pressure gas wells. Zhang et al.[11]studied the water hammer effect and its induced string vibration by using the method of mutual verification of theoretical modeling and simulation test. It is found that with the decrease of tubing diameter, the weight of tubing decreases and the diameter of tubing decreases. The damping effect is low, resulting in large pressure fluctuation and tubing string vibration. According to the fatigue failure mechanism of high-yield well tubing, Guo et al.[12]studied and established the fatigue life analysis method of high-yield well tubing string. Fluid-conveying pipes have been the subject of extensive research. Wang et al. suggested a nonlinear vibration fluid-conveying pipe model that included a vertical branch and a nonlinear vibration damage factor [13]. In addition to thoroughly examining the critical flow velocity and associated instability forms that could lead to pipeline collapse under four distinct boundary circumstances, Balkaya [14] illustrated the dynamic behavior of fluid-conveying pipelines under four distinct boundary conditions. The evolution of the in-plane and out-of-plane natural frequencies of curved microtubules under various flow velocity values and material length scale factors was investigated by Tang et al. [15], who also developed an in-plane and out-of-plane vibration analysis model for curved microtubules conveying fluid. At various points along the pipeline, ElNajjar and Daneshmand [16] talked about one or more extra masses or springs. The findings demonstrate that the critical flow rate can be raised by increasing the spring and point mass at a particular location. Eftekhari and Hosseini [17] developed the Rayleigh beam theory model of hollow thin walls and investigated the impact of fluid flow velocity and spin rate on the stable area. In addition to establishing the temperature-dependent partial differential equation, Mao et al. [18] examined the pertinent characteristics of the pipeline carrying fluid in the thermal environment, such as how temperature affects natural frequency and bending vibration. The pulsating coupling vibration of viscoelastic microtubes transporting pulsating fluid was investigated by Ghayesh et al. [19]. The parametric frequency response curves are acquired in the vicinity of the subcritical and supercritical critical speeds, close to the parametric resonance. The dynamic behavior of the pipeline under various conditions, including natural frequency, critical flow rate, and others, was examined by the researchers. Understanding the vibration characteristics of the pipe is to reduce those bad vibrations and reduce the harm.

Since composite pipes are widely used in the petroleum sector, some academics have been interested in the mechanical characteristics of composite pipes that are now in use. Maziar Mohammadzadeh et al. [20] used the full-order nonlinear equation obtained from the finite element method to study the dynamic properties of composite drill pipes under different drilling conditions as well as the effects of different fiber orientation angles and stacking sequences on the system. The mechanical characteristics of steel and composite risers were examined by Tan et al. [21] using the fluid-solid coupling analysis method. Composite risers were found to be more susceptible to vortex-induced vibration and to have lower structural frequencies. The FIV mechanism of composite tubing is currently poorly studied, and more research is required to fully understand the flow-induced vibration properties of composite tubing.

The internal fluid may cause the tube to vibrate or possibly fail due to fatigue. However, the medium in the tubing is mostly a gas-liquid two-phase mixture during the actual service process, which further complicates the vibration of the tubing coupling. The vibration

ISSN: 2688-8645

excitation mechanism in the transverse flow, including fluid elastic instability, periodic wake shedding, and random excitation, was described by Pettigrew and Taylor et al. [22]. They also discussed the effects of dynamic parameters such as hydrodynamic mass and damping on the vibration of the fluid-conveying pipe. By taking into consideration the effects of gravity, internal and external fluids, and bottom axial force, Wang et al. [23] developed a nonlinear mathematical model of drill string lateral vibration. The effects of gas concentration and annular fluid velocity on the lateral vibration of the drill string were examined by numerical simulation and experimental. Xu et al. [24] introduced a method for modeling a transient non-isothermal two-phase flow. The drift flow model describes the gas-liquid two-phase flow, and many transient energy conservation equations are used to forecast the temperature distribution of the drill pipe fluid, annulus fluid, casing string, and drill pipe. Ma and Gu et al. [25] investigated the dynamic behavior of the pipeline under the action gas-liquid two-phase internal flow using the Timoshenko beam model and the slip coefficient model. They discovered that the presence of two-phase flow will increase the pipeline's instability and have a greater effect on the system's dynamic response. At low gas flow rates, Kang et al. [26] investigated how gas-liquid two-phase flow in horizontal pipelines changed from laminar to turbulent flow. A numerical analysis of the vertical simply supported pipe model for gas-liquid two-phase internal flow transfer was conducted by Yun et al. [27]. It was discovered that the critical velocity would change either linearly or nonlinearly depending on changes in the dimensionless length-width ratio, dimensionless liquid volume, and dimensionless gravity coefficient. Chang et al[28]studied the in-line and cross-flow coupled vibration response characteristics of marine viscoelastic risers under the action of two-phase internal flow, which is affected by gas volume fraction, seawater flow rate, viscoelastic coefficient of marine risers, axial tension and other parameters.

There is no efficient dynamic model of composite tubing that takes into account gas-liquid-solid interaction, despite the fact that numerous specialists have examined the dynamic behavior of steel tubing in many different aspects. This research is innovative in that it examines the effects of gas-liquid internal flow velocity, gas volume fraction, bottom hole pressure, fiber orientation angle, and packer position on the vibration characteristics of composite tubing in a tubing system under the operation of numerous packers. Under the circumstances of gas-liquid two-phase internal flow, a dynamic model of composite tubing is suggested. The findings are thoroughly examined.

2. Dynamics Model of Composite Tubing

The gas-liquid two-phase internal flow composite tubing system under the influence of several packers is schematically depicted in Fig. 1. The following presumptions will be made in this work for the dynamic problem of the composite tubing system:

The impact of shear deformation is disregarded because of the composite oil pipe's enormous length-to-diameter ratio.

(1) The tube's fluid is uniform, non-rotating, non-viscous, incompressible, and does not take heat transmission into account.

(2) The collision between tubing and casing is not considered.

The composite tubing under the action of several packers can be reduced to a thin composite straight pipe subjected to gas-liquid two-phase internal flow, ignoring the influence of the assembly thread connection between the tubing and the tubing. The global coordinate system and the local coordinate system are respectively O_{xyz} and O_{1snz} , U_{fg} and U_{fL} represent the gas flow rate and the liquid flow rate in the multiphase internal flow respectively, θ represent the fiber direction angle. u, v respectively represent the displacement of any point on the composite tubing in the x, y directions.

Additionally, by consulting the pertinent theory of polar coordinates, the following connection can be learned for the thin-walled tube model with circular section.

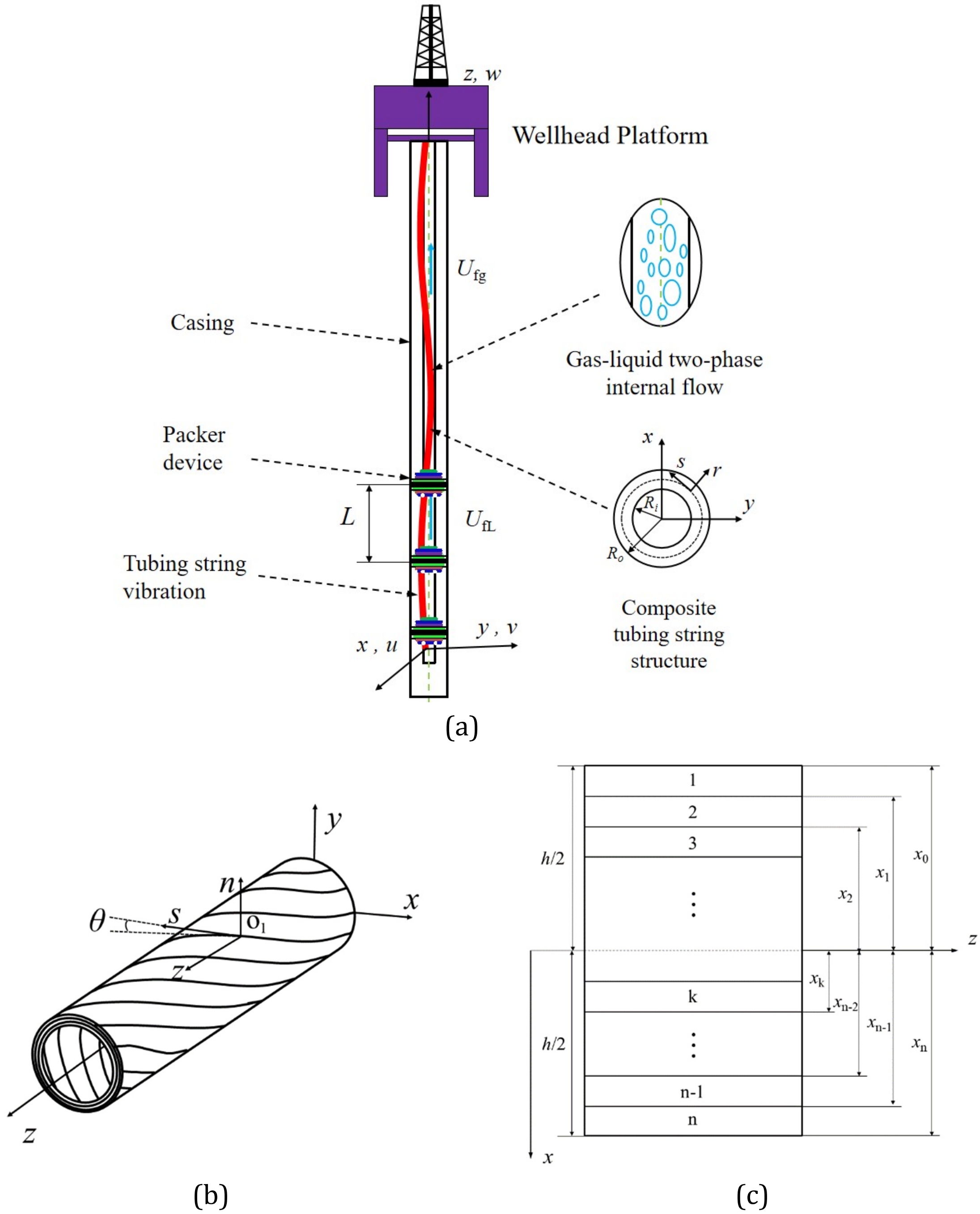

Fig 1. FIV model schematic diagram of composite tubing : (a) global coordinate system of composite tubing under two-phase internal flow ; (b) Composite tubing local coordinate system ; (c) Ply local schematic diagram

$$\frac{\mathrm{d}x}{\mathrm{d}s} = -\sin(\theta), \frac{\mathrm{d}y}{\mathrm{d}s} = \cos(\theta), \mathrm{d}s = R\mathrm{d}\theta \tag{1}$$

Based on the Kirchhoff hypothesis, the tube is thought to have minor deformation, per the literature of Bahaadini et al. [29]:

$$\begin{aligned} &\mathrm{u}(x,y,z;t)=u_0(z;t)\\ &v(x,y,z;t)=v_0(z;t)\\ &w(x,y,z;t)=-\frac{\partial v_0}{\partial z}\left[y(s)-n\frac{\mathrm{d}x}{\mathrm{d}s}\right]-\frac{\partial u_0}{\partial z}\left[x(s)+n\frac{\mathrm{d}y}{\mathrm{d}s}\right] \end{aligned} \tag{2}$$

Assuming the above, the Green's strain is:

$$\begin{aligned} &\varepsilon_{xx}=\frac{\partial u}{\partial x},\varepsilon_{yy}=\frac{\partial v}{\partial y},\varepsilon_{zz}=\frac{\partial w}{\partial z}+\frac{1}{2}\left[\left(\frac{\partial u}{\partial z}\right)^2+\left(\frac{\partial v}{\partial z}\right)^2\right],\\ &\varepsilon_{xz}=\frac{1}{2}\left(\frac{\partial u}{\partial z}+\frac{\partial w}{\partial x}\right),\varepsilon_{yz}=\frac{1}{2}\left(\frac{\partial v}{\partial z}+\frac{\partial w}{\partial y}\right),\varepsilon_{xy}=\frac{1}{2}\left(\frac{\partial u}{\partial y}+\frac{\partial v}{\partial x}\right) \end{aligned} \tag{3}$$

It can be acquired irrespective of the cross-sectional deformation of the tubing and the transverse shear effect:

$$\begin{aligned} &\varepsilon_{zz}=\varepsilon_{zz}^{(0)}+n\varepsilon_{zz}^{(n)},\quad \varepsilon_{zz}^{(0)}=-y(s)\frac{\partial^2 v_0}{\partial z^2}-x(s)\frac{\partial^2 u_0}{\partial z^2},\\ &\varepsilon_{zz}^{(1)}=\frac{\mathrm{d}x}{\mathrm{d}s}\frac{\partial^2 v_0}{\partial z^2}-\frac{\mathrm{d}y}{\mathrm{d}s}\frac{\partial^2 u_0}{\partial z^2}.\varepsilon_{zz}^{(2)}=\frac{\partial w_0}{\partial z}+\frac{1}{2}\left[\left(\frac{\partial u_0}{\partial z}\right)^2+\left(\frac{\partial v_0}{\partial z}\right)^2\right]. \end{aligned} \tag{4}$$

This work discusses the symmetrical distribution of the stacking mode of composite materials. When the composite layer is woven, the fiber's primary direction may not always match the tubing system's overall coordinates, x-y. It is assumed that θ is the angle between x-y and the material's primary direction. The stress-strain relationship is currently satisfied by the single-layer composite material.

$$\begin{bmatrix}\sigma_s\\ \sigma_z\\ \tau_{sz}\end{bmatrix}=\bar{\mathbf{Q}}\begin{bmatrix}\varepsilon_s\\ \varepsilon_z\\ \gamma_{sz}\end{bmatrix}=\begin{bmatrix}\bar{Q}_{11}&\bar{Q}_{12}&0\\ \bar{Q}_{12}&\bar{Q}_{22}&0\\ 0&0&\bar{Q}_{66}\end{bmatrix}\begin{bmatrix}\varepsilon_s\\ \varepsilon_z\\ \gamma_{sz}\end{bmatrix} \tag{5}$$

In the formula, σ_s,σ_z and τ_{sz} represent the normal stress and shear stress along the s-axis direction and the z-axis direction respectively, $\varepsilon_s,\varepsilon_z$, ε_{sz} represent the corresponding linear strain and shear strain respectively, $\bar{Q}_{ij}(i,j=1,2,6)$ represents the stiffness coefficient of the single-layer fiber material.

Slender tubing with thin walls has a very low circumferential stress, meaning that it is nil. Consequently, Eq. (5)'s parameter connection can be further stated as

$$\begin{aligned} &\varepsilon_s=-\frac{\bar{Q}_{12}}{\bar{Q}_{11}}\varepsilon_z,\\ &\sigma_z=\bar{Q}_{12}\varepsilon_s+\bar{Q}_{22}\varepsilon_z. \end{aligned} \tag{6}$$

Equation (5) can be substituted into equation (3) to yield the following expression for the tubing system's potential energy:

$$U=\frac{1}{2}\int_\Omega \sigma_z\varepsilon_z\mathrm{d}\Omega=\frac{1}{2}\int_0^L\oint_c\int_{-h/2}^{h/2}\left(\bar{Q}_{22}-\frac{\bar{Q}_{12}^2}{\bar{Q}_{11}}\right)\left(\varepsilon_z^{(0)}+n\varepsilon_z^{(1)}\right)^2\mathrm{d}n\mathrm{d}s\mathrm{d}z \tag{7}$$

Arranged

$$U=\frac{1}{2}\left(\bar{Q}_{22}-\frac{\bar{Q}_{12}^2}{\bar{Q}_{11}}\right)\int_0^L\oint_c\int_{-h/2}^{h/2}\begin{Bmatrix}\left[x^2+n^2\left(\frac{\mathrm{d}y}{\mathrm{d}s}\right)^2+2nx\frac{\mathrm{d}y}{\mathrm{d}s}\right]\left(\frac{\partial^2 u_0}{\partial z^2}\right)^2+\\ 2\left(xy-n^2\frac{\mathrm{d}x}{\mathrm{d}s}\frac{\mathrm{d}y}{\mathrm{d}s}+ny\frac{\mathrm{d}y}{\mathrm{d}s}-nx\frac{\mathrm{d}x}{\mathrm{d}s}\right)\left(\frac{\partial^2 u_0}{\partial z^2}\frac{\partial^2 v_0}{\partial z^2}\right)+\\ \left[y^2+n^2\left(\frac{\mathrm{d}x}{\mathrm{d}s}\right)^2-2ny\frac{\mathrm{d}x}{\mathrm{d}s}\right]\left(\frac{\partial^2 v_0}{\partial z^2}\right)^2\end{Bmatrix}\mathrm{d}n\mathrm{d}s\mathrm{d}z \tag{8}$$

By converting Eq. (8) into Eq. (1) and expressing the pertinent mathematical relationship using the stiffness coefficient, we can obtain

$$U=\frac{1}{2}\int_0^L\left\{a_{11}\left(\frac{\partial^2 u_0}{\partial z^2}\right)^2+a_{22}\left(\frac{\partial^2 v_0}{\partial z^2}\right)^2\right\}\mathrm{d}z \tag{9}$$

The stiffness coefficient, which is derived from the reference (Shadmehri et al[30].), is represented by the stiffness coefficients a_{11},a_{22} in the formula.

$$\begin{aligned}a_{11}&=\oint_c\left[K_{11}x^2+2K_{14}x\frac{\mathrm{d}y}{\mathrm{d}s}+K_{44}\left(\frac{\mathrm{d}y}{\mathrm{d}s}\right)^2\right]\mathrm{d}s,\\ a_{22}&=\oint_c\left[K_{11}y^2-2K_{14}y\frac{\mathrm{d}x}{\mathrm{d}s}+K_{44}\left(\frac{\mathrm{d}x}{\mathrm{d}s}\right)^2\right]\mathrm{d}s,\end{aligned} \tag{10}$$

And

$$\begin{aligned}&K_{11}=A_{22}-\frac{A_{12}^2}{A_{11}},K_{14}=D_{22}-\frac{B_{12}^2}{A_{11}},K_{44}=B_{22}-\frac{A_{12}B_{12}}{A_{11}},\\ &\left\{A_{ij},B_{ij},D_{ij}\right\}=\sum_{k=1}^{N}\int_{Z_k}^{Z_{k+1}}\bar{Q}_{ij}^{(k)}\left\{1,n,n^2\right\}\mathrm{d}n\quad i,j=1,2,6.\end{aligned} \tag{11}$$

The kinetic energy of the gas-liquid multiphase fluid in the pipe (T2) and the kinetic energy of the tubing itself (T1) make up the composite tubing system's kinetic energy. The exact phrase is as follows:

$$T=T_1+T_2 \tag{12}$$

Which

$$T_1=\frac{1}{2}\int_0^L\oint_c\int_{-h/2}^{h/2}\rho^{(k)}\left[\left(\frac{\partial u}{\partial t}\right)^2+\left(\frac{\partial v}{\partial t}\right)^2+\left(\frac{\partial w}{\partial t}\right)^2\right]\mathrm{d}n\mathrm{d}s\mathrm{d}z \tag{13}$$

$$\begin{aligned}T_2&=\frac{1}{2}m_i\int_0^L\left[{U_i}^2+\left(\frac{\partial u}{\partial t}+U_i\frac{\partial u}{\partial z}\right)^2+\left(\frac{\partial v}{\partial t}+U_i\frac{\partial v}{\partial z}\right)^2\right]\mathrm{d}z\\ &=\frac{1}{2}\int_0^L\begin{Bmatrix}m_{\mathrm{fg}}U_{\mathrm{fg}}^2+m_{\mathrm{fg}}\left(\frac{\partial u_0}{\partial t}+U_{\mathrm{fg}}\frac{\partial u_0}{\partial z}\right)^2+m_{\mathrm{fg}}\left(\frac{\partial v_0}{\partial t}+U_{\mathrm{fg}}\frac{\partial v_0}{\partial z}\right)^2+\\ m_{\mathrm{fL}}U_{\mathrm{fL}}^2+m_{\mathrm{fL}}\left(\frac{\partial u_0}{\partial t}+U_{\mathrm{fL}}\frac{\partial u_0}{\partial z}\right)^2+m_{\mathrm{fL}}\left(\frac{\partial v_0}{\partial t}+U_{\mathrm{fL}}\frac{\partial v_0}{\partial z}\right)^2\end{Bmatrix}\mathrm{d}z\end{aligned} \tag{14}$$

In the formula, L is the length of the composite tubing, $\rho^{(k)}$ is the density of the kth layer composite material of the tubing, m_{fg} and m_{fL} represent the gas phase mass and liquid phase mass per unit length in the tubing, respectively. m_{v} is the mass of composite tubing per unit length, and the specific expression is as follows.

$$m_{\mathrm{v}} = \sum_{k=1}^{N} \oint_c \int_{z_k}^{z_{k+1}} \rho^{(k)} \mathrm{d}n \mathrm{d}s \tag{15}$$

Likewise, by representing the pertinent mathematical relationship with the stiffness coefficient, it can be determined that

$$T_1 = \frac{1}{2}\int_0^L m_{\mathrm{v}} \left\{ \left(\frac{\partial u_0}{\partial t}\right)^2 + \left(\frac{\partial v_0}{\partial t}\right)^2 + \left(\frac{\partial w_0}{\partial t}\right)^2 + b_{22}\left(\frac{\partial^2 u_0}{\partial z \partial t}\right)^2 + b_{33}\left(\frac{\partial^2 v_0}{\partial z \partial t}\right)^2 \right\} \mathrm{d}z \tag{16}$$

Which

$$\begin{gathered}
\left(b_0, b_1, b_2\right) = \sum_{k=1}^{N} \int_{z_k}^{z_{k+1}} \rho^{(k)} \left(1, n, n^2\right) \mathrm{d}n, \\
b_{22} = \oint_c \left[b_0 x^2 + 2 b_1 x \frac{\mathrm{d}y}{\mathrm{d}s} + b_2 \left(\frac{\mathrm{d}y}{\mathrm{d}s}\right)^2 \right] \mathrm{d}s, \\
b_{33} = \oint_c \left[b_0 y^2 - 2 b_1 y \frac{\mathrm{d}x}{\mathrm{d}s} + b_2 \left(\frac{\mathrm{d}x}{\mathrm{d}s}\right)^2 \right] \mathrm{d}s
\end{gathered} \tag{17}$$

Furthermore, the work performed in the tubing system by non-conservative factors such external forces and structural damping is given as

$$W = \int_0^L \left[F_x u_0 - c\frac{\partial u_0}{\partial t} u_0 + F_y v_0 - c\frac{\partial v_0}{\partial t} v_0 - \frac{1}{2}F_z\left(\frac{\partial u_0}{\partial t}\right)^2 - \frac{1}{2}F_z\left(\frac{\partial v_0}{\partial t}\right)^2 - c\frac{\partial w_0}{\partial t} w_0 \right] \mathrm{d}z \tag{18}$$

In the formula, c is the damping coefficient, F_x and F_y are the lateral forces in the X and Y directions of the tubing, respectively. The effective axial force F_z can be expressed as

F_x and F_y represent the lateral forces in the X and Y directions of the tube, respectively, and c is the damping coefficient in the formula. The expression for the effective axial force E is

$$F_z = F - \left(m_{\mathrm{v}} + m_{\mathrm{fg}} + m_{\mathrm{fL}}\right) \mathrm{g} \left(L - z\right) \tag{19}$$

In the formula, F represents the bottom hole pressure of coiled tubing. g denotes the acceleration of gravity.

According to Hamilton 's principle, the kinetic energy, potential energy and the work done by the non-conservative force of the tubing system have the following relationship.

$$\delta \int_{t_1}^{t_2} \left(T - U\right) \mathrm{d}t + \int_{t_1}^{t_2} \delta W \mathrm{d}t = 0 \tag{20}$$

It should be emphasized that the stress-strain relationship of the single-layer fiber of the composite tubing in the coordinate with an angle of θ to the main direction of the material is expressed as

$$\begin{bmatrix} \sigma_1 \\ \sigma_2 \\ \tau_{12} \end{bmatrix} = \mathbf{Q} \begin{bmatrix} \varepsilon_1 \\ \varepsilon_2 \\ \gamma_{12} \end{bmatrix} = \begin{bmatrix} Q_{11} & Q_{12} & 0 \\ Q_{12} & Q_{22} & 0 \\ 0 & 0 & Q_{66} \end{bmatrix} \begin{bmatrix} \varepsilon_1 \\ \varepsilon_2 \\ \gamma_{12} \end{bmatrix} \tag{21}$$

where σ_1, σ_2 and τ_{12} stand for the shear stress along the main direction and the normal stress, respectively. The linear strain and shear strain in the primary direction are represented, respectively, by $\varepsilon_1, \varepsilon_2$ and ε_{12}.

The stress rotation axis formula can be used to express the relationship between the transformation matrix $\overline{Q}$ in the formula and the two-dimensional stiffness matrix Q of the tubing in the formula.. The specific expression is

$$\bar{\mathbf{Q}} = \mathbf{T}_t^{-1}\mathbf{Q}\left(\mathbf{T}_t^{-1}\right)^T \tag{22}$$

The specific expression of the coordinate transformation matrix T_t is

$$\mathrm{T}_t = \begin{bmatrix} \cos^2\theta & \sin^2\theta & 2\sin\theta\cos\theta \\ \sin^2\theta & \cos^2\theta & -2\sin\theta\cos\theta \\ -\sin\theta\cos\theta & \sin\theta\cos\theta & \cos^2\theta - \sin^2\theta \end{bmatrix} \tag{23}$$

Therefore, the specific expression of each parameter in the matrix $\overline{Q}^{(k)}$ in the kth layer of the composite tubing is

$$\begin{aligned}
\overline{Q}_{11}^{(k)} &= Q_{11}^{(k)}\cos^4\theta + 2(Q_{12}^{(k)} + 2Q_{66}^{(k)})\sin^2\theta\cos^2\theta + Q_{22}^{(k)}\sin^4\theta, \\
\overline{Q}_{12}^{(k)} &= (Q_{11}^{(k)} + Q_{22}^{(k)} - 4Q_{66}^{(k)})\sin^2\theta\cos^2\theta + Q_{12}^{(k)}(\sin^4\theta + \cos^4\theta), \\
\overline{Q}_{22}^{(k)} &= Q_{11}^{(k)}\sin^4\theta + 2(Q_{12}^{(k)} + 2Q_{66}^{(k)})\sin^2\theta\cos^2\theta + Q_{22}^{(k)}\cos^4\theta, \\
\overline{Q}_{66}^{(k)} &= (Q_{11}^{(k)} + Q_{22}^{(k)} - 2Q_{12}^{(k)} - 2Q_{66}^{(k)})\sin^2\theta\cos^2\theta + Q_{66}^{(k)}(\sin^4\theta + \cos^4\theta).
\end{aligned} \tag{24}$$

In the formula, $\overline{Q}_{ij}^{(k)}$ is the stiffness coefficient of the two-dimensional stiffness matrix in the kth layer of the composite tubing, and its specific expression is

$$Q_{11}^{(k)} = \frac{E_{11}}{1 - \dfrac{E_{22}}{E_{11}}\nu_{12}^2}, Q_{12}^{(k)} = \frac{\nu_{12}E_{12}}{1 - \dfrac{E_{22}}{E_{11}}\nu_{12}^2}, Q_{22}^{(k)} = \frac{E_{22}}{1 - \dfrac{E_{22}}{E_{11}}\nu_{12}^2}, Q_{66}^{(k)} = G_{12} \tag{25}$$

This work considers the viscoelastic model and replaces the Hamiltonian equation with the aforementioned equation. The following are the vibration control formulae for two-way composite tubing under gas-liquid multiphase internal flow:

$$\begin{aligned}
&\left(m_v + m_{fg} + m_{fl}\right)\frac{\partial^2 u_0}{\partial t^2} - b_{22}\frac{\partial^4 u_0}{\partial z^2\partial t^2} + a_{11}\left(1 + \alpha_1\frac{\partial}{\partial t}\right)\frac{\partial^4 u_0}{\partial z^4} + c\frac{\partial u_0}{\partial t} \\
&+\left(2m_{\mathrm{fg}}U_{\mathrm{fg}} + 2m_{\mathrm{fL}}U_{\mathrm{fL}}\right)\frac{\partial^2 u_0}{\partial t\partial z} + \left(m_{\mathrm{fg}}U_{\mathrm{fg}}^2 + m_{\mathrm{fL}}U_{\mathrm{fL}}^2\right)\frac{\partial^2 u_0}{\partial z^2} - \frac{\partial}{\partial z}\left(T_{\mathrm{e}}\frac{\partial u_0}{\partial z}\right) + F_x = 0 \\
&\left(m_v + m_{fg} + m_{fl}\right)\frac{\partial^2 u_0}{\partial t^2} - b_{33}\frac{\partial^4 v_0}{\partial z^2\partial t^2} + a_{22}\left(1 + \alpha_1\frac{\partial}{\partial t}\right)\frac{\partial^4 v_0}{\partial z^4} + c\frac{\partial v_0}{\partial t} \\
&+\left(2m_{\mathrm{fg}}U_{\mathrm{fg}} + 2m_{\mathrm{fL}}U_{\mathrm{fL}}\right)\frac{\partial^2 v_0}{\partial t\partial z} + \left(m_{\mathrm{fg}}U_{\mathrm{fg}}^2 + m_{\mathrm{fL}}U_{\mathrm{fL}}^2\right)\frac{\partial^2 v_0}{\partial z^2} - \frac{\partial}{\partial z}\left(T_{\mathrm{e}}\frac{\partial v_0}{\partial z}\right) + F_y = 0
\end{aligned} \tag{26}$$

The boundary of the tube end connection constraint between the lower end and the upper end of the tubing is simplified to simply supported, and the boundary condition is expressed as

$$\begin{aligned}
&u_0(0,t) = 0,\ a_{11}\frac{\partial^2 u_0}{\partial z^2}(0,t) = 0,\ u_0(L,t) = 0,\ a_{11}\frac{\partial^2 u_0}{\partial z^2}(L,t) = 0 \\
&v_0(0,t) = 0,\ a_{22}\frac{\partial^2 v_0}{\partial z^2}(0,t) = 0,\ v_0(L,t) = 0,\ a_{22}\frac{\partial^2 v_0}{\partial z^2}(L,t) = 0
\end{aligned} \tag{27}$$

In order to facilitate the research, the work of the relevant parameter reference in the gas-liquid multiphase internal flow model in this paper. The multiphase internal flow is described by the slip state of gas and liquid in the tube. Based on the volume flow rate, the gas volume per unit length of the tubing is defined as C_{fg}, the liquid volume per unit length of the tubing is defined as C_{fL}, the gas volume flow rate is defined as Q_{fg}, and the liquid volume flow rate is Q_{fL}. The porosity α_2, gas volume fraction ε_g and slip coefficient K are expressed as

$$\alpha_2 = \frac{C_{\mathrm{fg}}}{C_{\mathrm{fg}} + C_{\mathrm{fL}}}, \quad \varepsilon_{\mathrm{g}} = \frac{Q_{\mathrm{fg}}}{Q_{\mathrm{fg}} + Q_{\mathrm{fL}}}, \quad K = \frac{U_{\mathrm{fg}}}{U_{\mathrm{fL}}} \tag{28}$$

In addition, the slip coefficient K can also be expressed as a function of porosity α_2 and gas volume fraction ε_g.

$$K = \frac{1-\alpha_2}{\alpha_2} = \left(\frac{\varepsilon_{\mathrm{g}}}{1-\varepsilon_{\mathrm{g}}}\right)^{1/2} \tag{29}$$

In the formula, ρ_g is the gas phase internal flow density of the tubing, and ρ_L is the liquid phase internal flow density of the tubing.

3. Model Solution

For the convenience of research, the following dimensionless parameters are introduced into the coupled vibration model of composite tubing.

$$\begin{cases} \left(\xi, u_0^*, v_0^*, w_0^*\right) = \dfrac{\left(z, u_0, v_0, w_0\right)}{L}, \quad \left(k_1, k_2\right) = \dfrac{\left(a_{11}, a_{22}\right)}{E_{11} I} \\ \tau = \dfrac{t}{L^2}\sqrt{\dfrac{E_{11}I}{m}}, \ \alpha = \dfrac{m_{\mathrm{fg}}}{m_v + m_{fg} + m_{fL}}, \ \beta = \dfrac{m_{\mathrm{fL}}}{m_v + m_{fg} + m_{fL}}, \ U_{\mathrm{g}}^* = \sqrt{\dfrac{m_{\mathrm{fg}}}{E_{11}I}} U_{\mathrm{fg}} L, \\ U_L^* = \sqrt{\dfrac{m_{\mathrm{fL}}}{E_{11}I}} U_{\mathrm{fL}} L, \ \upsilon = \dfrac{m_{\mathrm{v}}}{m_v + m_{fg} + m_{fL}}, \ \left(\mu_1, \mu_2\right) = \dfrac{\left(b_{22}, b_{33}\right)}{mL^2}, \ \gamma = \sqrt{\dfrac{E_{11}I}{m}} \dfrac{\alpha_1}{L^2}, \\ \sigma = \dfrac{cL^2}{\sqrt{E_{11}Im}}, \ \left(\lambda_1, \lambda_2, \lambda_3\right) = \dfrac{(F_x, F_y, F_z)L^3}{E_{11}I}, P^* = \dfrac{FL^3}{E_{11}I}, \\ ,\Omega_{\mathrm{s}} = \omega_{\mathrm{s}} L^2 \sqrt{\dfrac{m}{E_{11}I}}, F^* = \dfrac{\left(m_{\mathrm{v}} + m_{\mathrm{fg}} + m_{\mathrm{fL}}\right) g L^3}{E_{11}I}, \end{cases} \tag{30}$$

The nonlinear dimensionless flow-induced vibration partial differential equation of the composite tubing can be obtained by substituting the dimensionless stiffness parameter into the vibration equation obtained above, ignoring the nonlinear term and the external force term of the equation.

$$\begin{aligned} &\frac{\partial^2 u_0^*}{\partial \tau^2} - \mu_1 \frac{\partial^4 u_0^*}{\partial \xi^2 \partial \tau^2} + k_1 \frac{\partial^4 u_0^*}{\partial \xi^4} + k_1 \gamma \frac{\partial^5 u_0^*}{\partial \xi^4 \partial \tau} + \sigma \frac{\partial u_0^*}{\partial \tau} + 2\left(\sqrt{\alpha} U_{\mathrm{g}}^* + \sqrt{\beta} U_{\mathrm{L}}^*\right) \frac{\partial^2 u_0^*}{\partial \xi \partial \tau} + \\ &\left[\left(U_{\mathrm{g}}^*\right)^2 + \left(U_{\mathrm{L}}^*\right)^2 - P^* + F^*\left(1-\xi\right)\right] \frac{\partial^2 u_0^*}{\partial \xi^2} - F^* \frac{\partial u_0^*}{\partial \xi} = 0 \end{aligned} \tag{31}$$

$$\begin{aligned} &\frac{\partial^2 v_0^*}{\partial \tau^2} - \mu_2 \frac{\partial^4 v_0^*}{\partial \xi^2 \partial \tau^2} + k_2 \frac{\partial^4 v_0^*}{\partial \xi^4} + k_2 \gamma \frac{\partial^5 v_0^*}{\partial \xi^4 \partial \tau} + \sigma \frac{\partial v_0^*}{\partial \tau} + 2\left(\sqrt{\alpha} U_{\mathrm{g}}^* + \sqrt{\beta} U_{\mathrm{L}}^*\right) \frac{\partial^2 v_0^*}{\partial \xi \partial \tau} + \\ &\left[\left(U_{\mathrm{g}}^*\right)^2 + \left(U_{\mathrm{L}}^*\right)^2 - P^* + F^*\left(1-\xi\right)\right] \frac{\partial^2 v_0^*}{\partial \xi^2} - F^* \frac{\partial v_0^*}{\partial \xi} = 0 \end{aligned} \tag{32}$$

u_0^*, v_0^* are continuous variables, so the solution of the linear control equation is in the form of

$$u_0^*\left(\xi,\tau\right)=\sum_{j=1}^{N}\varphi_j(\xi)q_j(\tau),\quad v_0^*\left(\xi,\tau\right)=\sum_{j=1}^{N}\varphi_j(\xi)q_j(\tau) \tag{33}$$

$\varphi_j(\xi)$ is the trial function in the equation above. The trial function in this case is the modal function of the simply supported beam. The coordinate of generalized time is $q_j(\tau)$. N stands for both the discrete order of Galerkin and the number of degrees of freedom. The computed result is near to the actual answer when N is large. Since N cannot be infinite, the residual $R[\eta,\xi]$, which represents the exact answer in the solution process, must contain an error. The weight function is chosen as the trial function itself in accordance with the Galerkin approach, and the weighted average value of the residual value within the continuum's range is 0.

$$\int_0^1\varphi_i\left(\xi\right)R\left[\eta,\xi\right]\mathrm{d}\xi=0, i=1,2,\cdots N \tag{34}$$

The linear control equation can be further deduced.

$$\begin{cases}\sum_{j=1}^{N}\Big[\int_0^1\varphi_i(\xi)\varphi_j(\xi)\mathrm{d}\xi\cdot\ddot{q}_j(\tau)-\mu_1\int_0^1\varphi_i(\xi)\varphi_j(\xi)''\mathrm{d}\xi\cdot\ddot{q}_j(\tau)+k_1\gamma\int_0^1\varphi_i(\xi)\varphi_j(\xi)''''\mathrm{d}\xi\cdot\dot{q}_j(\tau)\\ +\sigma\int_0^1\varphi_i(\xi)\varphi_j(\xi)\mathrm{d}\xi\cdot\dot{q}_j(\tau)+2\left(\sqrt{\alpha}U_\mathrm{g}^*+\sqrt{\beta}U_\mathrm{L}^*\right)\int_0^1\varphi_i(\xi)\varphi_j(\xi)'\mathrm{d}\xi\cdot\dot{q}_j(\tau)\\ +k_1\int_0^1\varphi_i(\xi)\varphi_j(\xi)''''\mathrm{d}\xi\cdot q_j(\tau)+\left[\left(U_\mathrm{g}^*\right)^2+\left(U_\mathrm{L}^*\right)^2\text{-}P^*+F\left(1-\xi\right)\right]\int_0^1\varphi_i(\xi)\varphi_j(\xi)''\mathrm{d}\xi\cdot q_j(\tau)\\ \text{-}F^*\int_0^1\varphi_i(\xi)\varphi_j(\xi)'\mathrm{d}\xi\cdot q_j(\tau)=0\end{cases} \tag{35}$$

Since MATLAB programming calculations are required for the linear component of the solution analysis, the above formula must be simplified into a matrix form. The structural control equation matrix is

$$\left[M\right]\left\{\ddot{q}\right\}+\left[C\right]\left\{\dot{q}\right\}+\left[K\right]\left\{q\right\}=0 \tag{36}$$

In the above formula

$$\{\boldsymbol{q}\}=\left[q_1,q_2,\cdots q_N\right]^T$$

$$\boldsymbol{M}=\left[m_{ij}\right],m_{ij}=\int_0^1\varphi_i(\xi)\varphi_j(\xi)\mathrm{d}\xi-\mu_1\int_0^1\varphi_i(\xi)\varphi_j(\xi)''\mathrm{d}\xi$$

$$\boldsymbol{C}=\left[c_{ij}\right],c_{ij}=k_1\gamma\int_0^1\varphi_i(\xi)\varphi_j(\xi)''''\mathrm{d}\xi+\sigma\int_0^1\varphi_i(\xi)\varphi_j(\xi)\mathrm{d}\xi$$

$$+2\left(\sqrt{\alpha}U_\mathrm{g}^*+\sqrt{\beta}U_\mathrm{L}^*\right)\int_0^1\varphi_i(\xi)\varphi_j(\xi)'\mathrm{d}\xi$$

$$\boldsymbol{K}=\left[k_{ij}\right],k_{ij}=k_1\int_0^1\varphi_i(\xi)\varphi_j(\xi)''''\mathrm{d}\xi+\left[\left(U_\mathrm{g}^*\right)^2+\left(U_\mathrm{L}^*\right)^2\text{-}P^*+F\left(1-\xi\right)\right]\int_0^1\varphi_i(\xi)\varphi_j(\xi)''\mathrm{d}\xi$$

$$\text{-}F^*\int_0^1\varphi_i(\xi)\varphi_j(\xi)'\mathrm{d}\xi$$

Through the boundary conditions, assuming that the Galerkin discrete modal function is

$$\varphi_i(\xi)=\sqrt{2}\sin\left(i\xi\pi\right) \tag{37}$$

The generalized mass, damping, and stiffness matrices are obtained by substituting the form of the control equation's solution into the linear equation as follows:

$$\left[M\right]\left\{\ddot{\eta}\right\}+\left[C\right]\left\{\dot{\eta}\right\}+\left[K\right]\left\{\eta\right\}=0 \tag{38}$$

The solution of the above equation can be further written as

$$\left\{\eta\right\}=\left\{\overline{\eta}\right\}\exp(\omega_*\tau) \tag{39}$$

Furthermore, it can be obtained

$$\left(\omega_*^2\left[\bar{M}\right]+\omega_*\left[\bar{C}\right]+\left[\bar{K}\right]\right)\{\bar{\eta}\}=0 \tag{40}$$

The solution of the above formula can be transformed into finding the generalized eigenvalue of the equation. The obtained result is the frequency ω^* of the system, and the natural frequency depends on the imaginary frequency of the system.

$$E_g=\begin{bmatrix} \boldsymbol{0} & \boldsymbol{I} \\ -\bar{M}^{-1}\bar{K} & -\bar{M}^{-1}\bar{C} \end{bmatrix} \tag{41}$$

4. Numerical Results and Discussion

In this section, the effects of gas volume fraction, fiber orientation angle, bottom hole pressure and different positions of packer on the vibration characteristics of tubing are analyzed by numerical results. In the following calculation, we specify the geometric parameters as shown in the following Table1 and Table2.

Table 1. Values for geometry and physical properties of composite tubing of string[32]

Parameters	Description	Value
D_i	Inner diameter	0.25
N_n	Number of layers of the composite tubing of string	8
H	Fiber layer thickness(m)	0.002
α_1	Viscoelastic structural damping coefficient	0.001
ρ_{fL}	Density of fluid-phase internal flow(kg/m^3)	880
ρ_{fg}	Density of gas-phase internal flow(kg/m^3)	1.293
P	Material density of tubing of string	1601

Table 2. Material characteristic parameter values of composite tubing of string[32]

Parameters	Description	Value
E_{11}	Elastic modulus(GPa)	137
E_{22}	Elastic modulus	9
G_{12}	Shear modulus	3.8
V_{12}	Poisson ratio	0.3

4.1. Validation of the Method

In order to verify the validity and accuracy of the dynamic model and calculation method, the calculation in this paper is compared with that of Ni et al.[31].When $\mu_1=0,k_1=0,\sigma=0,\gamma=0,\varepsilon_g=0,P^*=0,F^*=0$ the model is a single-phase flow tubing model without considering the composite material, internal and external flow damping, and the system 's own gravity and bottom hole pressure. The natural frequency and critical velocity of the system are calculated in this state. The accuracy of the degradation model is known by comparison with the literature.

In order to further verify the effectiveness and accuracy of the dynamic model of the tubing with composite materials and two-phase flow, the model is compared with the article of Chang et al [32].At this time, $\varepsilon_g=0.5,P^*=25,\theta=60°$, the model is a dynamic model of the two-phase flow tubing considering the composite material and the bottom hole pressure. In this state, the natural frequency and critical flow rate of the composite tubing system are calculated. By comparing with the literature, the accuracy of the dynamic model proposed in this paper can be known.

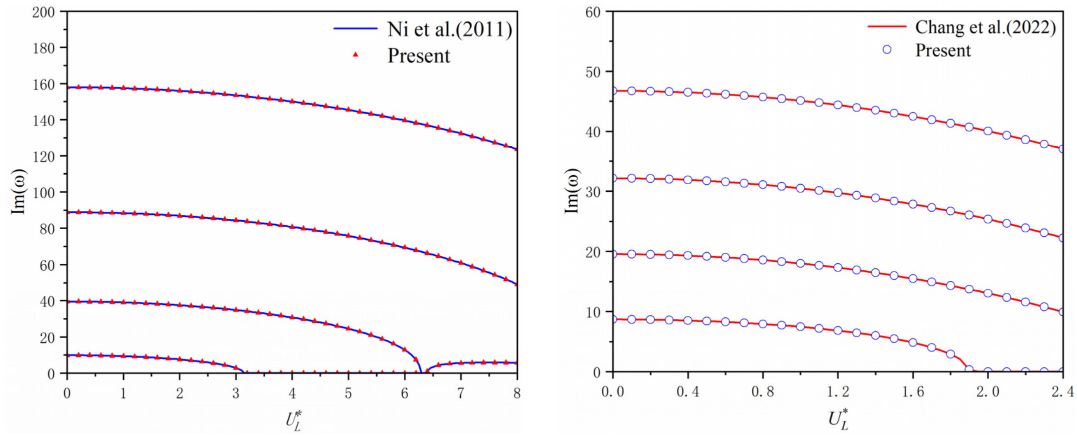

(a) (b)

Fig 2. The first four order natural frequency verification ; (a) Degradation model validation (b) Composite material model validation with two-phase internal flow

4.2. Effect of Gas Volume Fraction on Vibration Characteristics of Tubing

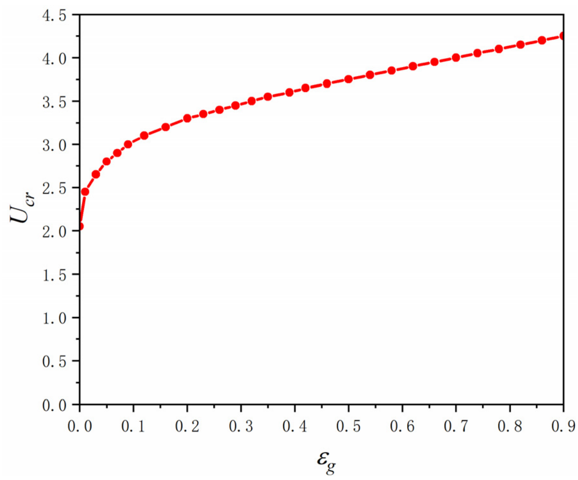

Fig 3. Relationship between critical flow rate and gas volume fraction

The above figure describes the change of the critical flow rate of the composite tubing with the gas volume fraction. It can be seen from the above figure that when the gas volume fraction A, the gas volume fraction has a great influence on the critical flow rate. When A, it can be seen that the critical flow rate of the system changes linearly with the gas volume fraction. In addition, it can also be seen from the above diagram that the critical flow rate of the system increases from B = 0 when B = 0 to B = 0 when B = 0, and the critical flow rate increases by nearly 2.5 times. In practical engineering applications, the critical flow rate of the tubing can be roughly judged according to the gas volume fraction at the oil well work site.

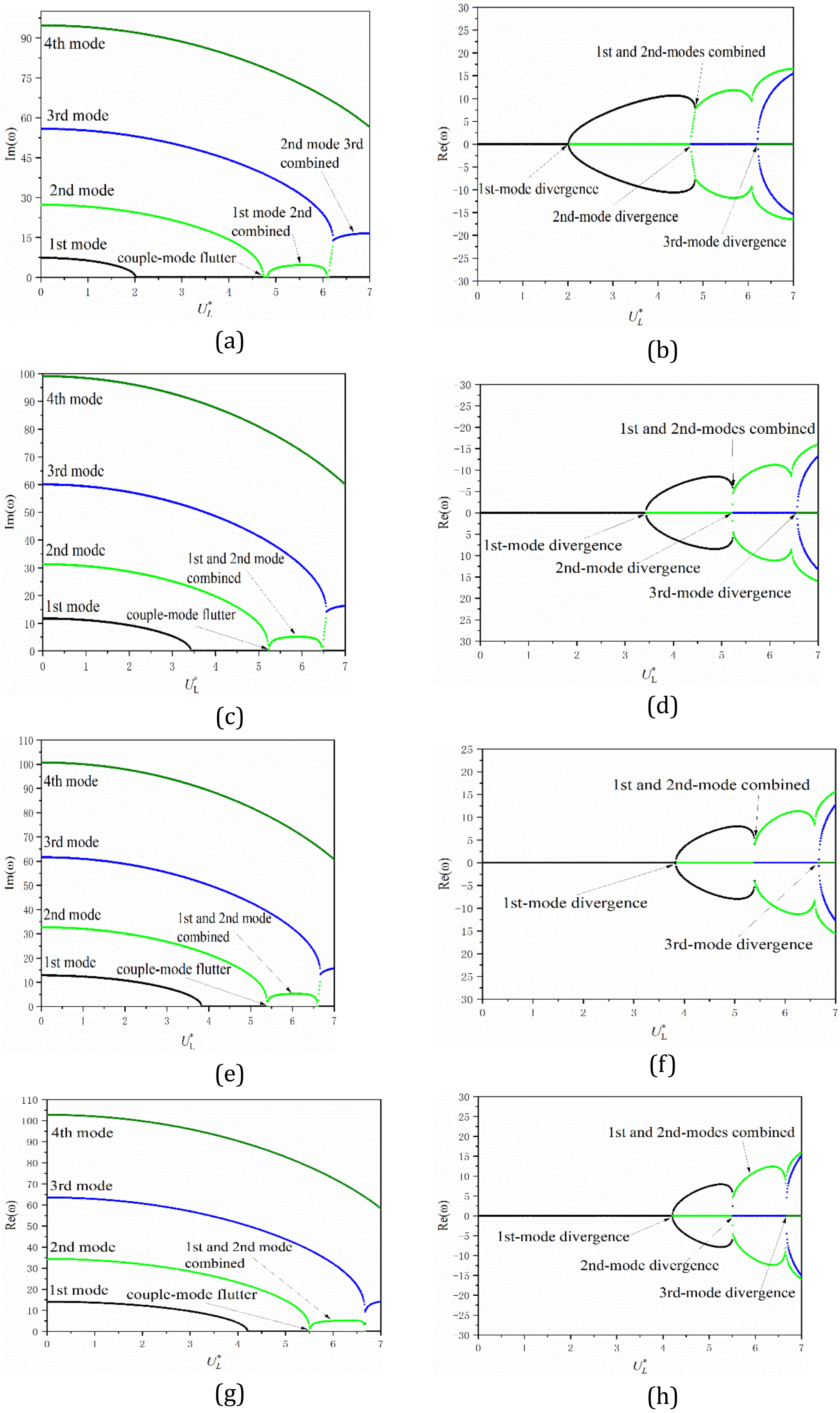

Fig 4. Relationship between liquid velocity and frequency under different volume fraction distributions

In Fig.4, the real and imaginary frequencies of the system under different gas volume fractions are shown from a to j, respectively. Through the analysis of these real and imaginary frequencies, the stability interval of the pipeline can be obtained. When the flow rate is 0, it can be seen from the real part frequency diagram that the real part frequency is 0, and the modes of the fourth-order real part frequency are coupled. In the form of the solution in this paper, the real component of the complex frequency $\mathrm{Re}(\omega)$ represents the increase or decay of the vibration response, while the imaginary part represents the intrinsic frequency $\mathrm{Im}(\omega)$ of the pipe vibration. The real and imaginary components of the system's complex frequency can be used to assess the stability of the system. When $\mathrm{Im}(\omega)>0$, $\mathrm{Re}(\omega)=0$, the system is in a stable state; when $\mathrm{Im}(\omega)=0$, $\mathrm{Re}(\omega)<0$, the system is in static instability; when $\mathrm{Im}(\omega)>0$, $\mathrm{Re}(\omega)<0$, the system is in dynamic instability. For Figure 4, the qualitative analysis is carried out from the trend of the frequency diagram. It can be seen from Figure 4 (a) (b) that when the mass ratio of the gas is 0, the first-order natural frequency decreases slowly with the increase of the flow rate. In the range of dimensionless flow rate from 2.02 to 4.74, the natural frequency is 0. It means that in this flow rate range, the pipeline will spontaneously vibrate without external excitation. After exceeding the flow rate in this interval, the natural frequency begins to increase. And the first-order natural frequency and the second-order natural frequency are coupled when the dimensionless flow rate is 4.74, and the second-order natural frequency and the third-order natural frequency are coupled when the dimensionless flow rate is 6.22. At this time, the imaginary part of the complex frequency is positive, and the real part of the complex frequency is negative, indicating that the system has a coupled dynamic instability. At the beginning of the real part frequency, the fourth-order frequency is coupled with the increase of the dimensionless flow rate and begins to slowly decouple from the coupling state. When the flow rate is 2.02, the first-order and second-order real part frequencies and the flow rate are 4.73, the second-order and third-order real part frequencies begin to decouple and gradually develop into different curve shapes. It can be seen from Fig.4 (c) (d) that when $\varepsilon_{\mathrm{g}}=0.3$, the first-order modal instability occurs when the dimensionless flow rate is 3.44, and the coupled dynamic instability occurs when the dimensionless flow rate is 5.23. It can be seen from Fig.4 (e) (f) that when $\varepsilon_{\mathrm{g}}=0.6$, the first-order modal instability occurs when the dimensionless flow rate is 3.83, and the coupled dynamic instability occurs when the dimensionless flow rate is 5.4. It can be seen from Fig.4 (g) (h) that when $\varepsilon_{\mathrm{g}}=0.9$, the first-order modal instability occurs when the dimensionless flow rate is 4.20, and the coupled dynamic instability occurs when the dimensionless flow rate is 5.51. In different gas volume fractions ε_{g}, when $U_L^*<5.02$, the oil and gas pipeline system will not undergo coupled dynamic instability. Moreover, the above analysis shows that the gas volume fraction T of the two-phase flow has a great influence on the natural frequency and critical velocity of the system.

Figure 5 shows the change of the first four natural frequencies of the system with the flow rate and the gas volume fraction ε_{g}. It can be seen from figure 5(a) that when $U_L^*=0,\varepsilon_g=0.9$,the frequency $\omega=14.06$ of the first order mode. When $U_L^*=2.05,\varepsilon_g=0$, the frequency $\omega=0$ of the first mode. That is, the point with the highest frequency appears at the position where the flow rate is low and the gas volume fraction is high, while the point with the lowest frequency appears at the position where the flow rate is high and the gas volume fraction is minimum. From figure 5, it can also be seen that the change of flow velocity has a great influence on the low-order modal frequency at $\varepsilon_{\mathrm{g}}<0.2$, and has little influence on the low-order modal frequency at $\varepsilon_{\mathrm{g}}>0.2$, and the change of gas volume fraction has a great influence on the low-order modal frequency at $\varepsilon_{\mathrm{g}}<0.2$, and has little influence on the low-order modal frequency at

$\varepsilon_g > 0.2$. However, for high-order frequencies, both flow velocity and volume fraction have a great influence on the frequency. This is because the gas volume fraction will affect the mass ratio, thus affecting the natural frequency and critical flow rate of the system.

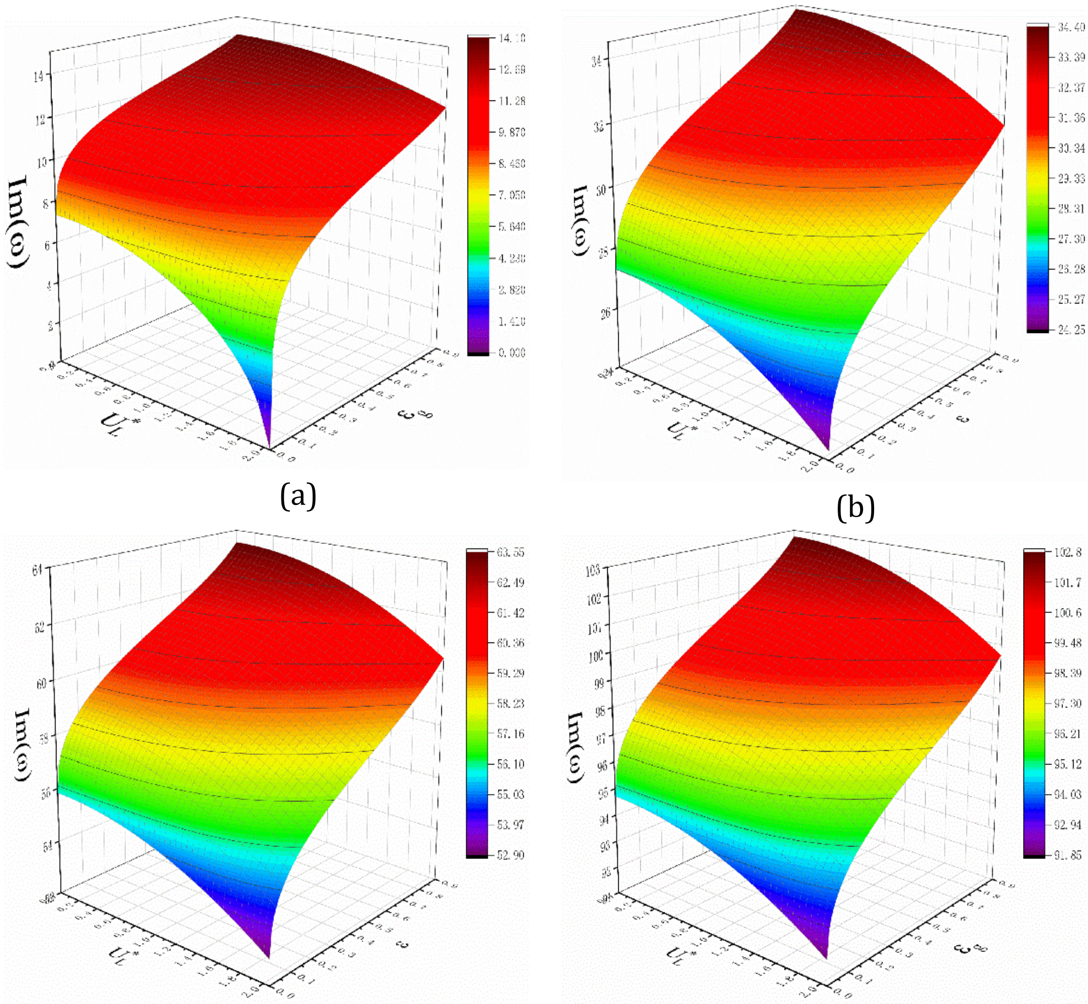

Fig 5. Variations of the modal frequencies of the system with liquid velocity and ε_g .(a)1st natural frequencies,(b) 2nd natural frequencies,(c) 3rd natural frequencies,(d) 4th natural frequencies.

4.3. Effect of Fiber Orientation Angle on Vibration Characteristics of Tubing

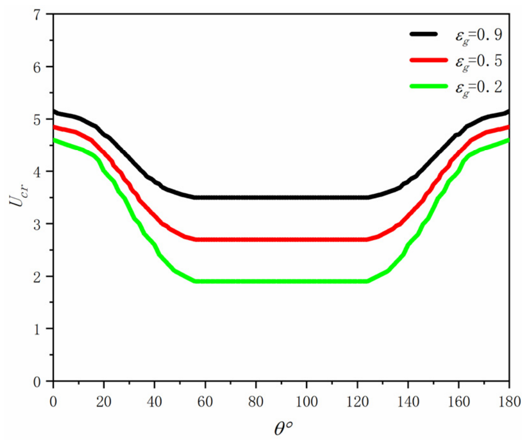

Fig 6. Relationship between fiber orientation angle and critical flow velocity and $P^* = 25, U_L^* = 0.7$

Fig.6 is a schematic diagram of the critical flow rate of the composite tubing with the change of the fiber orientation angle. It can be seen from the figure that the critical flow rate changes little with the fiber orientation angle in the interval $0^{\circ} < \theta < 20^{\circ}$.At $20^{\circ} < \theta < 56^{\circ}$, the critical flow rate of the composite tubing system has a significant downward trend. With the change of fiber orientation angle, the critical flow rate of the system will not change in the interval of $56^{\circ} < \theta < 124^{\circ}$, and remain a constant value. In addition, it is not difficult to see from the diagram that the curve of the critical flow rate of the system with the change of fiber orientation angle is symmetrically distributed.

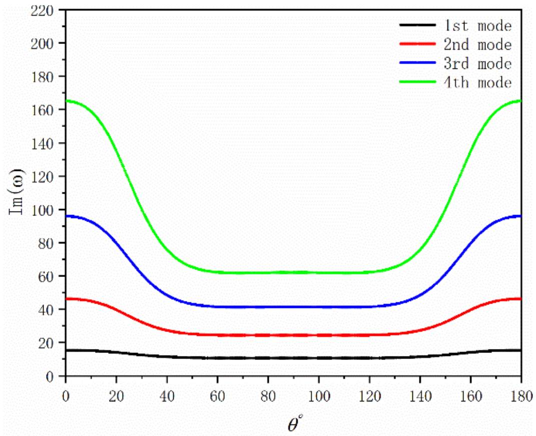

Fig 7. The relationship between the natural frequency of the system and the fiber orientation angle and $\varepsilon_g = 0.5, P^* = 25, U_L^* = 0.7$

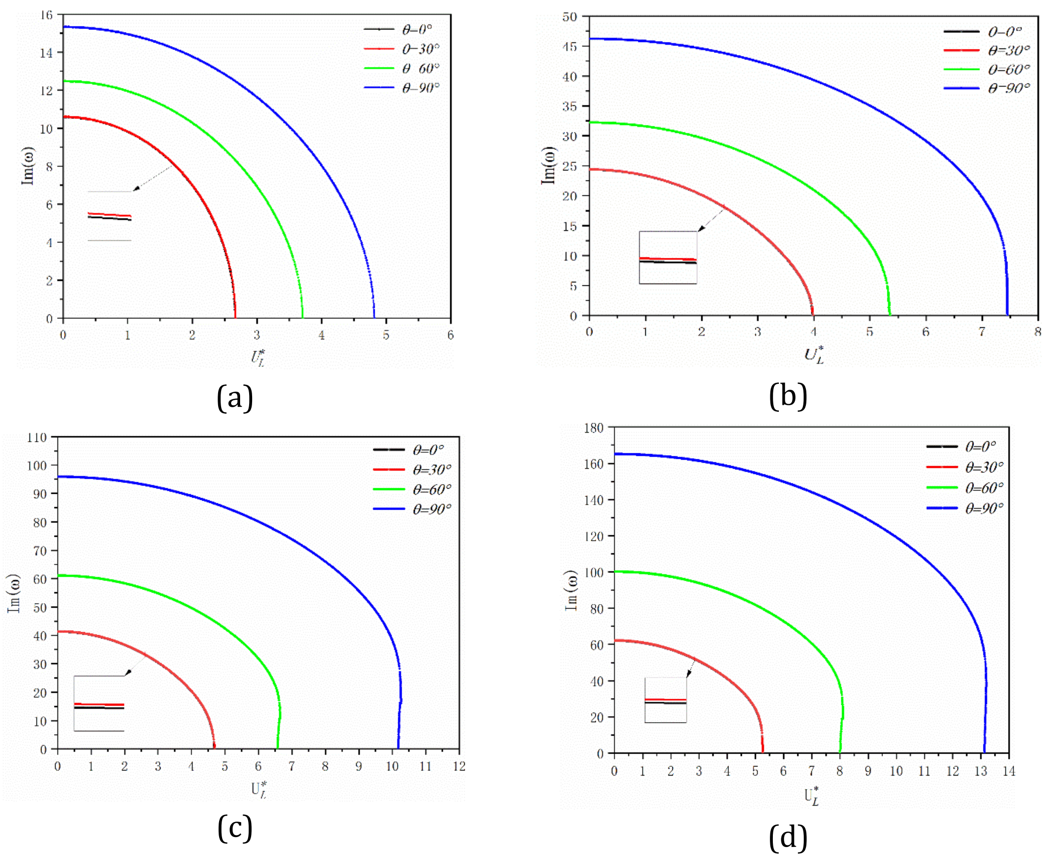

Fig 8. Relationship between natural frequency and liquid velocity. (a)1st natural frequencies,(b) 2nd natural frequencies,(c) 3rd natural frequencies,(d) 4th natural frequencies

It can be seen from Fig.7 that the natural frequency of the tubing changes nonlinearly with $\theta = 90^{\circ}$ as the symmetry axis as the fiber orientation angle increases. Among them, when $0^{\circ} < \theta < 5^{\circ}$, the natural frequency of the tubing changes little with the fiber orientation angle. When $5^{\circ} < \theta < 56^{\circ}$, the natural frequency of the tubing decreases faster, especially the high-order natural frequency decreases more obviously. When $5^{\circ} < \theta < 56^{\circ}$, the natural frequency of the tubing is almost unaffected by the fiber orientation angle and remains at a certain value.

Figure 8 is a schematic diagram of the first four natural frequencies changing with the liquid flow rate under different fiber orientation angles. From the diagram (a) (b) (c) (d), it can be seen that the first four natural frequencies decrease nonlinearly with the liquid flow rate, and whether it is low-order mode or high-order mode, when the fiber orientation angle is sum, the natural frequency change curve of the system almost overlaps.

4.4. Effect of Bottom Hole Pressure on Tubing Vibration Characteristics

During the service of tubing, it is usually in a high temperature and high pressure environment. When there is a large bottom hole pressure acting on the composite tubing, it will lead to buckling failure of the tubing string. Therefore, it is necessary to study the vibration characteristics of the tubing in view of the bottom hole pressure.

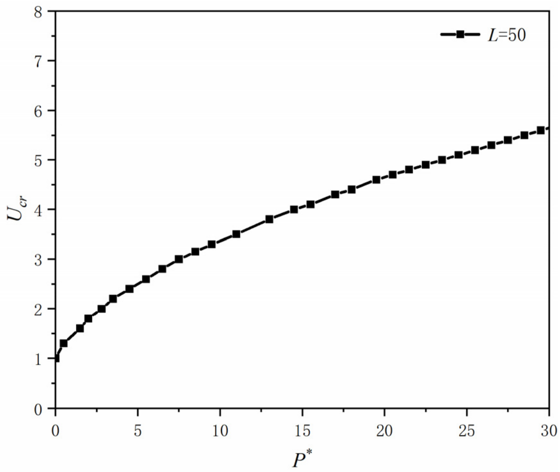

Fig 9. Relationship between bottom hole pressure and critical flow velocity

Fig. 9 is a schematic diagram of the composite tubing system changing with the bottom hole pressure. It can be seen from the diagram that when L = 50, the critical flow rate of the system increases nonlinearly with the bottom hole pressure, and the curve is a smooth curve.

Figure 10 is the first four order natural frequency curve of composite tubing under different bottom hole pressure. The qualitative analysis of the trend of the frequency diagram above shows that at $\varepsilon_g = 0$, the first-order natural frequency of the composite tubing system is 0 in the range of dimensionless bottom hole pressure of 0 to 27.5. It means that in this dimensionless bottom hole pressure range, the composite tubing will spontaneously vibrate without external excitation. This is because when the dimensionless bottom hole pressure is small, its value is much smaller than the tubing weight, resulting in buckling instability under the weight. When the dimensionless bottom hole pressure exceeds 27.5, the natural frequency of the composite tubing rises nonlinearly. This is because the increased bottom hole pressure will increase the stiffness of the tubing, which will increase the natural frequency of each order of the tubing. It can be seen from the figure that with the increase of gas volume fraction, the tubing system is more sensitive to bottom hole pressure. In addition, it can be seen from the diagram that the influence of dimensionless bottom hole pressure on high-order frequency is

ISSN: 2688-8645

less than that of low-order frequency. In particular, it can be seen from the fourth-order frequency that the natural frequency of the tubing system changes almost linearly with the change of bottom hole pressure.

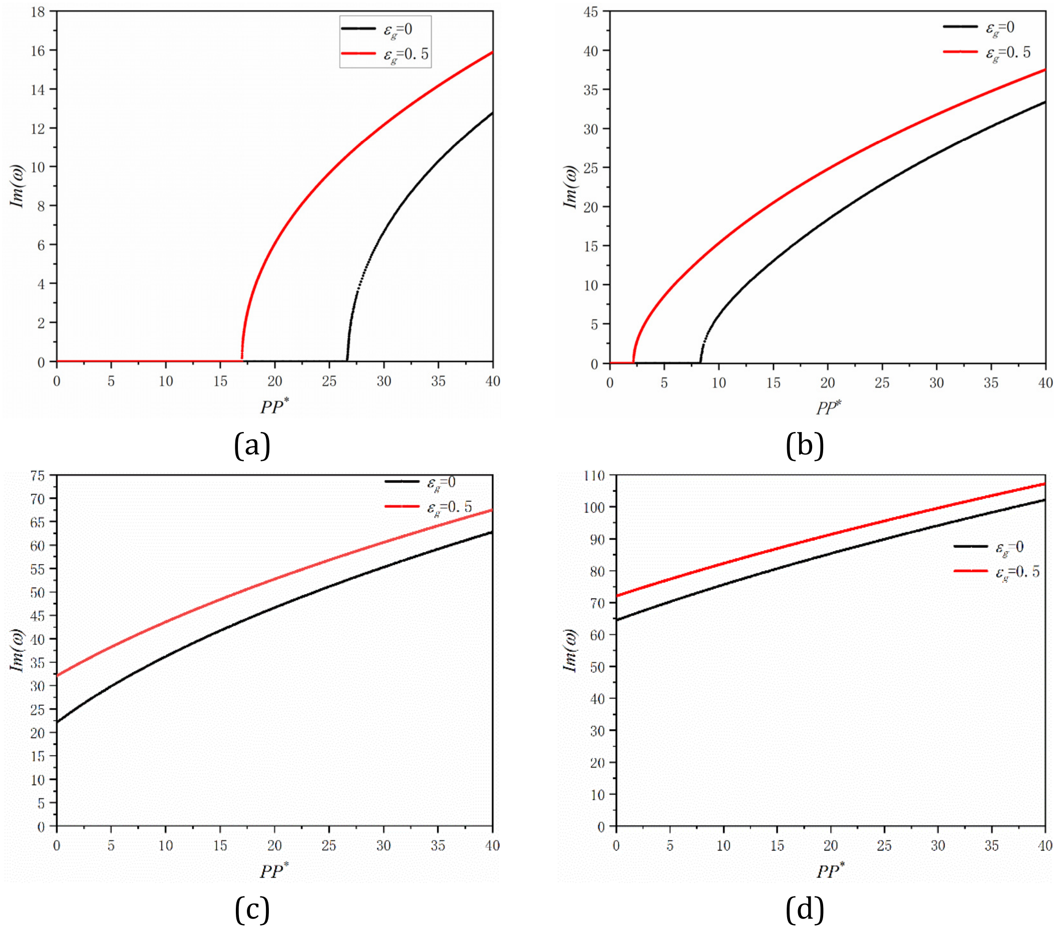

Fig 10. The relationship between the first four natural frequencies of the system and the dimensionless bottom hole pressure. (a)1st natural frequencies,(b) 2nd natural frequencies,(c) 3rd natural frequencies,(d) 4th natural frequencies.

4.5. The Influence of Different Installation Positions of Packer on the Vibration Characteristics of Tubing

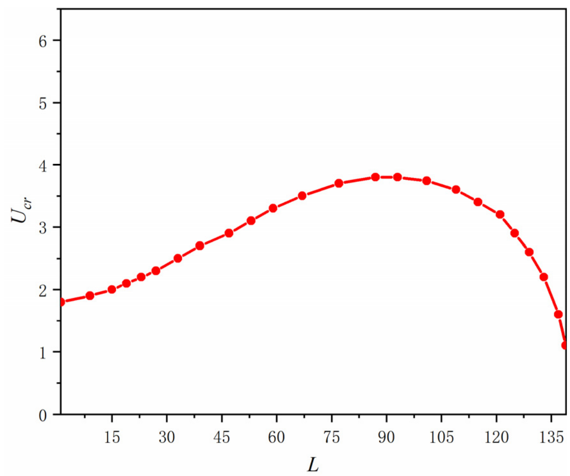

Fig 11. Relationship between tubing critical flow velocity and packer position

ISSN: 2688-8645

Fig.11 is a schematic diagram of the critical flow rate of the composite tubing system changing with the different installation positions of the packer. It can be seen from Fig.11 that the critical flow rate of the system changes nonlinearly with the position of the packer, and the change curve appears at L = 90. The extreme point, that is, the critical flow rate of the system in the interval of $1 < L < 90$ increases nonlinearly with the increase of L, reaches the maximum at L = 90, and decreases nonlinearly with the increase of L at L > 90.

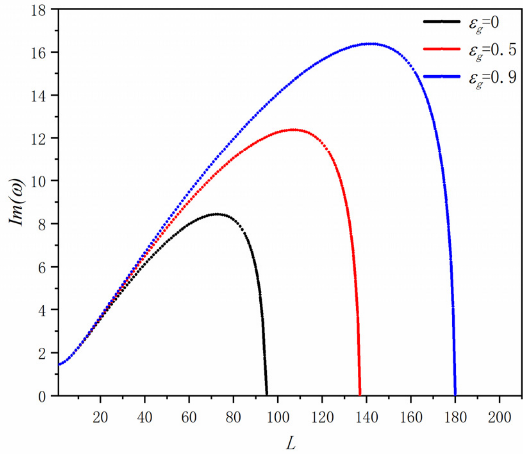

(a)

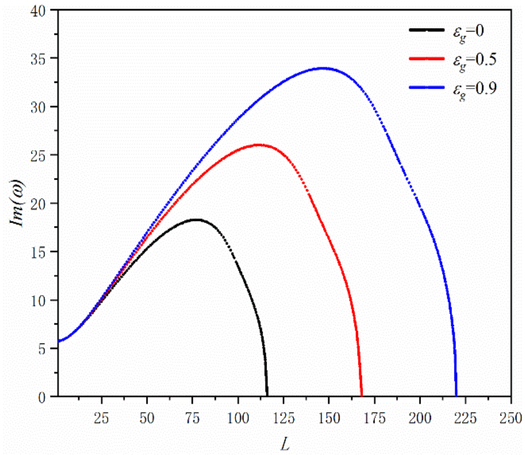

(b)

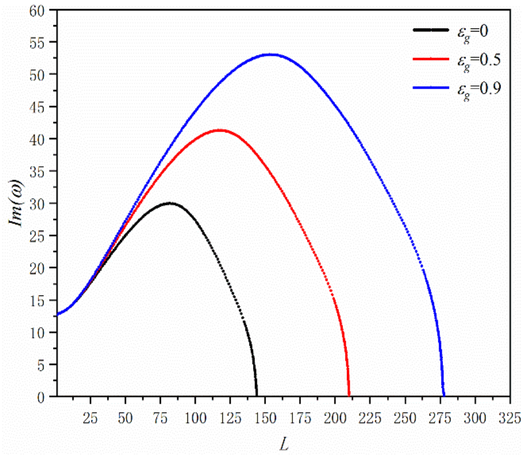

(c)

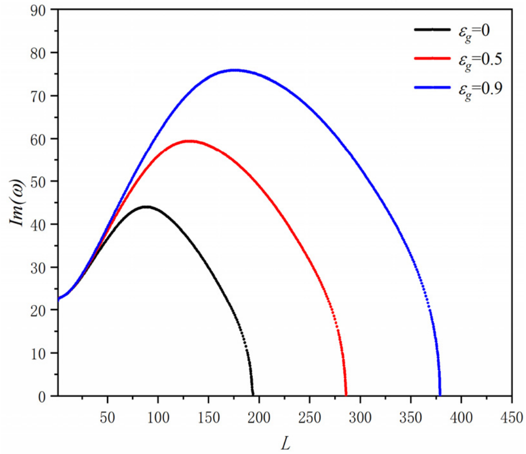

(d)

Fig 12. The relationship between the first four natural frequencies of the system and the position change of the packer. (a)1st natural frequencies,(b) 2nd natural frequencies,(c) 3rd natural frequencies,(d) 4th natural frequencies.

Figure 12 is the curve of the natural frequency of the composite tubing with the position of the packer. Firstly, the qualitative analysis of Figure 10 from the trend of the frequency diagram is carried out. It can be seen from Fig.11 (a) (b) (c) (d) that the three curves almost coincide in the interval range of $1 < L < 50$, indicating that the gas volume fraction ε_g has little effect on the natural frequency of the system with the change of the packer position in this interval. With the increase of L, the three curves develop into different curves. In addition, with the increase of L, there will be an extreme point in the natural frequency of the system. After the L value exceeds the extreme point, the natural frequency of the system decreases nonlinearly with L. Among them, the change of L in the nonlinear decline interval is more sensitive to the low-order natural frequency, while the high-order frequency decreases slowly with the change of L.

5. Conclusion

This paper mainly studies the vibration characteristics of composite tubing under the action of gas-liquid two internal flow. The effects of gas volume fraction, fiber orientation angle, bottom hole pressure in oil and gas wells and packer position on the vibration characteristics of composite tubing were studied. These results are helpful to deepen the understanding of the flow-induced vibration law of gas-liquid two-phase internal flow composite tubing, and provide theoretical basis and technical support for the dynamic design and optimization of composite tubing. By calculating the numerical results of the model, it is found that the increase of gas volume fraction can significantly improve the critical flow rate of the system, and at $\varepsilon_g > 0.2$, the critical flow rate changes linearly with the gas volume fraction. With the increase of fiber orientation, the critical flow velocity of the tubing system will not change when the fiber orientation angle is in the range of $56^\circ < \theta < 124^\circ$. With the increase of the bottom hole pressure, it is found that the natural frequency of the tubing will increase nonlinearly with the bottom hole pressure. This is because the increase of the bottom hole pressure will increase the stiffness of the tubing, and then increase the natural frequency of each order of the tubing, and the increase of the bottom hole pressure can significantly improve the critical flow rate of the system. In addition, it is found that the different installation positions of the packer have a great influence on the vibration characteristics of the tubing. The critical flow velocity of the tubing system changes nonlinearly with the position of the packer, and there will be a maximum value at a certain position. When the packer position is $1 < L < 50$, the change of gas volume fraction has little effect on the natural frequency of the system, and with the increase of the packer position, the natural frequency of the system will also appear an extreme point.

Data Availability Statement

The datasets generated during this study are fully available within the article and supplementary materials.

Declaration of Competing Interest

We declare that we have no financial and personal relationships with other people or organizations that can inappropriately influence our work, there is no professional or other personal interest of any nature or kind in any product, service and/or company that could be construed as influencing the position presented in, or the review of, the manuscript entitled.

Acknowledgments

This research work has been supported in part by National Natural Science Foundation of China (Grant Nos. 51674216) and Fellowship of China Postdoctoral Science Foundation (No. 2022M712643). This research are also supported by Key R & D projects of Sichuan Province (Grant No. 2022YFQ0034) and Natural Science Foundation Project of Sichuan Province (Grant No. 2022NSFSC1922).

References

[1] A, M. G. , B, K. B. K. , A, P. P. , C, V. J. , C, J. L. , & C, N. D. . (2017). Hybrid composite tensile armour wires in flexible risers: a multi-scale model. Composite Structures, 162, 13-27.

[2] Hastie, J. C. , Guz, I. A. , & Kashtalyan, M. . (2019). Effects of thermal gradient on failure of a thermoplastic composite pipe (tcp) riser leg. International Journal of Pressure Vessels & Piping, 172, 90-99.

[3] Yang, M ;Ma, Y; Li, SG. (2012).Vibration Characteristics Analysis of Tubing String in Three-High Gas Well[J].Advanced Materials Research, Vol.455-456: 395-399.

[4] Aitken, J. (1878). XIV. An account of some experiments on rigidity produced by centrifugal force. The London, Edinburgh, and Dublin Philosophical Magazine and Journal of Science, 5(29), 81–105.

[5] Shilling, R., III, and Lou, Y. K. (1980).An Experimental Study on the Dynamic Response of a Vertical Cantilever Pipe Conveying Fluid. ASME. *J. Energy Resour. Technol*. September 1980; 102(3): 129–135.

[6] Guo, Xiao qiang;Li, Xiao;Liu, Jun;Dai, Liming;Huang, Liang;Wei, Anchao;Zhang, Xiaohong. (2021).Fatigue failure mechanism of 3D tubing strings used in high-pressure, high-temperature and high-yield curved gas wells.[J].Engineering Failure Analysis, Vol.128: 105536.

[7] Wang, Y. , Fan, H. , Zhang, L. P. , & Yang, H. . (2011). An analysis of axial tubing vibration in a high-pressure gas well. Liquid Fuels Technology, 29(7), 708-714.

[8] Wickert, J. A. . (1992). Non-linear vibration of a traveling tensioned beam. J. of Non-Linear Mechanics, 27(3), 503-517.

[9] Yu, K. Q. (2017). Fluid solid coupling vibration analysis and safety evaluation of completion string of high production gas well. **'an University of petroleum.

[10] Guo, X., Liu, J., Wang, G., Dai, L., Fang, D., Huang, L., & He, Y. (2021). Nonlinear flow-induced vibration response characteristics of a tubing string in HPHT oil&gas well. Applied Ocean Research, 106, 102468.

[11] Zhang, Q., Liao, T., Ding, L., Wang, K., Yang, H., & Lian, Z. (2023). Study on water hammer effect and tubing string vibration in high-pressure high-production gas wells. Geoenergy Science and Engineering, 229, 212147.

[12] Guo, X., Liu, J., Dai, L., He, Y., Huang, L., Wang, G., & Yu, L. (2021). Fatigue investigation of tubing string in high-yield curved wells. Journal of Natural Gas Science and Engineering, 85, 103688.

[13] Wang, X. Y., Zhou, Z., Liu, X. P. (2013). Numerical analysis of the vibration of pipes conveying fluid under the influence of vertical branch. Advanced Materials Research, 655, 620-624.

[14] Balkaya, M., Kaya, M. O. (2021).Analysis of the instability of pipes conveying fluid resting on two-parameter elastic soil under different boundary conditions. Ocean Engineering.241, 110003.

[15] Tang, M., Ni, Q., Wang, L., Luo, Y., Wang, Y. (2014).Nonlinear modeling and sizedependent vibration analysis of curved microtubes conveying fluid based on modified couple stress theory. International Journal of Engineering Science. 84,1–10.

[16] ElNajjar, J., Daneshmand, F. (2020). Stability of horizontal and vertical pipes conveying fluid under the effects of additional point masses and springs. Ocean Engineering. 206,106943.

[17] Eftekhari, M., Hosseini, M. (2016).On the stability of spinning functionally graded cantilevered pipes subjected to fluid-thermomechanical loading.International Journal of Structural Stability and Dynamics. 16,1550062.

[18] Mao, X. Y., Gao, S. Y., Ding, H., Chen, L. Q. (2023). Static bifurcation and nonlinear vibration of pipes conveying fluid in thermal environment.Ocean Engineering. 278,114418.

[19] Ghayesh, M. H., Farokhi, H., Farajpour, A. (2019).Pulsatile vibrations of viscoelastic microtubes conveying fluid. Microsystem Technologies,.25, 3609-3623.

[20] Maziar Mohammadzadeh;Mohammadreza Arbabtafti;Majid Shahgholi & Jianming Yang.(2022). Nonlinear vibrations of composite drill strings considering drill string–wellbore contact and bit–rock interaction[J].Archive of Applied Mechanics. Vol.92(9): 2569-2592.

[21] Tan, L. B., Chen, Y., Jaiman, R. K., Sun, X., Tan, V. B. C., & Tay, T. E. (2015). Coupled fluid–structure simulations for evaluating a performance of full-scale deepwater composite riser. Ocean Engineering, 94, 19-35.

[22] Pettigrew, M. J., and Taylor, C. E. (1994). "Two-Phase Flow-Induced Vibration: An Overview (Survey Paper)." ASME. *J. Pressure Vessel Technol*. August 1994; 116(3): 233–253.

[23] Wang B, Wang L, Meng X, Ren F. 2023. Effect of Annular Gas–Liquid Two-Phase Flow on Lateral Vibration of Drill String in Horizontal Drilling for Natural Gas Hydrate. *Processes*. 11(1):54.

[24] Xu, Zhengming; Song, Xianzhi; Li, Gensheng; Wu, Kan; Pang, Zhaoyu; Zhu, Zhao peng. 2018.Development of a transient non-isothermal two-phase flow modelfor gas kick simulation in HTHP deep well drilling[J].Applied Thermal Engineering. Vol.141(1): 1055-1069.

[25] Ma, T., Gu, J. & Duan, M. (2017). Dynamic response of pipes conveying two-phase flow based on Timoshenko beam model. *Mar Syst Ocean Technol* **12**, 196–209.

[26] Kang, J., Zhang, X., Zhang, D., & Liu, Y. (2021). Pressure drops and mixture friction factor for gas–liquid two-phase transitional flows in a horizontal pipe at low gas flow rates. *Chemical Engineering Science*, *246*, 117011.

[27] Gao, Y., Liu, L., Fu, S., Chai, S., & Shi, C. (2023). Nonlinear dynamics of a vertical pipe subjected to a two-phase, solid-liquid internal flow. *Applied Mathematical Modelling*, *120*, 651-666.

[28] Xueping Chang;Jinming Fan;Wenwu Yang and Yinghui Li. (2021).In-Line and Cross-Flow Coupling Vibration Response Characteristics of a Marine Viscoelastic Riser Subjected to Two-Phase Internal Flow[J].Shock and Vibration. Vol.2021(1): 1-27.

[29] Bahaadini, Reza;Dashtbayazi, Mohammad Reza;Hosseini, Mohammad;Khalili-Parizi, Zahra. 2018.Stability analysis of composite thin_walled pipes conveying fluid.[J].Ocean Engineering. Vol.160: 311-323.

[30] F. Shadmehri;B. Derisi;S.V. Hoa;(2011).On bending stiffness of composite tubes[J].Composite Structures. Vol.93(9): 2173-2179.

[31] Ni, Q., Zhang, Z. L., & Wang, L. (2011). Application of the differential transformation method to vibration analysis of pipes conveying fluid. *Applied Mathematics and Computation*, *217*(16), 7028-7038.

[32] Chang, X. P., Qu, C. J., Song, Q., Li, Y. H., & Liu, J. (2022). Coupled cross-flow and in-line vibration characteristics of frequency-locking of marine composite riser subjected to gas-liquid multiphase internal flow. *Ocean Engineering*, *266*, 113019.